InAsSb-based nBn photodetectors: lattice mismatched growth on GaAs and low-frequency noise performance.

A. P. Craig,[1] M. D. Thompson,[1] Z.-B. Tian,[2] S. Krishna,[2] A. Krier,[1] and A. R. J. Marshall,[1]

[1]Physics Department, Lancaster University, Lancaster LA1 4YB, United Kingdom

[2]Center for High Technology Materials, Department of Electrical and Computer Engineering, University of New Mexico, Albuquerque, NM 87106, USA

Abstract

An InAsSb nBn detector structure was grown on both GaAs and native GaSb substrates. Temperature dependent dark current, spectral response, specific detectivity (D^*) and noise spectral density measurements were then carried out. Shot-noise-limited D^* figures of 1.2×10^{10} Jones and 3.0×10^{10} Jones were calculated (based upon the sum of dark current and background photocurrent) for the sample grown on GaAs and the sample grown on GaSb, respectively, at 200 K. Noise spectral density measurements revealed knee frequencies of between 124-337 Hz and ~8 Hz, respectively. Significantly, these devices could support focal plane arrays capable of operating under thermoelectric cooling.

nBn photodetectors are known to offer reduced dark currents and noise when compared with simple *p-i-n* photodiodes.[1,2] Through the use of a barrier layer which blocks the dark currents due to the flow of majority carriers, but allows the flow of photogenerated holes, the *nBn* detector is essentially a hybrid between photoconductor and photodiode. The dark currents are further known to be dominated by the diffusion current alone, even at low temperatures, due to an inherent suppression of Shockley-Read-Hall (SRH) currents.[2,3] This effect is attributed to the confinement of the electric field within the barrier layer, away from the narrow-bandgap absorption and contact layers, which are strongly susceptible to SRH generation and band-to-band tunnelling. Furthermore, *n*-type doping in these regions, whether unintentional or extrinsic, pins the Fermi-level at the conduction band edge, away from mid-bandgap traps associated with SRH generation. Surface currents are also inhibited by the *nBn* design, especially if the barrier layer is not etched when defining the mesas in processing, leading to a high shunt resistance. This is particularly significant since the surface currents of InAsSb *p-i-n* diodes tend to dominate at low temperatures (at least without optimised passivation). *nBn* detectors were initially grown using absorption layers of bulk-material InAs,[1] but progress has been made with *nBn* structures using absorption layers consisting of InAsSb,[2,3] quaternaries,[4] and strained-layer-superlattices. The latter have been implemented both in a straightforward manner, using the type-II InAs/GaSb system,[5-7] as well as using a two-colour design, with two absorption regions (with different superlattice periods) allowing sensitivity in more than one spectral range.[8] Initial reports of *nBn* detectors created using the HgCdTe material system have also surfaced.[9,10] While focal plane arrays for infrared cameras – whether for defence,[11] security or other purposes – are expected to be the primary application for *nBn* detector based sensors, further applications in gas sensing[12] and environmental monitoring are also noteworthy, among others. The reduced cooling requirements[1] of *nBn* detectors are their key benefit: these are often significant enough that

compact and cost effective thermoelectric coolers can be used. This is particularly attractive when portability is a concern, e.g. on the battlefield. The first sensors based on *nBn* detectors have recently become available commercially.13 In this letter, progress in the growth and characterisation of InAsSb-based *nBn* detectors is reported. A detector structure was grown, both lattice-mismatched on GaAs, using the interfacial misfit (IMF) array growth mode, and on native GaSb. Full details of the IMF growth mode may be found elsewhere.14,15 Comparisons were made between these two primary samples using Arrhenius plots of the dark currents and temperature dependent spectral response and specific detectivity (D*) measurements. Two further samples were then grown to allow for an investigation of the effects of the absorption region doping concentration upon device characteristics. Finally, the frequency dependence of the noise spectrum was measured for the two primary samples

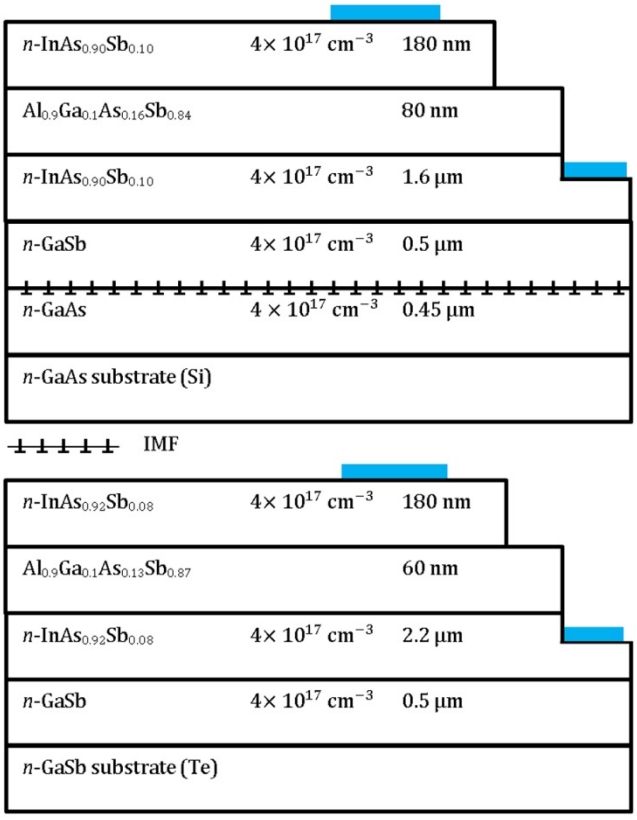

Figure 1: Layer thicknesses and compositions for the two primary samples. Top: growth on a GaAs substrate (via an IMF array). Bottom: growth on native a GaSb substrate.

to check for the presence of 1/f noise and determine the range of frequencies affected.

Details of the two structures are shown in Figure 1. All growth was performed using a VG V80-H MBE reactor. For the sample grown on GaAs, oxide desorption was performed first at 600 °C, followed by growth of the GaAs buffer layer at 570 °C. The IMF interface was next initiated by closing the As valve for a short interval, cooling the sample to 510 °C under Sb_2 flux and then opening the Ga cell shutter. A thin GaSb buffer layer was then grown at 510 °C. The ternary absorption layer was grown at 450 °C with an extrinsic *n*-type doping level of $\sim 4 \times 10^{17}$ cm^{-3}. The GaTe dopant cell was calibrated beforehand using Hall Effect measurements. The quaternary barrier layer (grown at 490 °C) was unintentionally doped (expected to be $\sim 10^{16}$ cm^{-3} *p*-type, based on values for binary AlSb)16 and included a 10% Ga mole fraction, suppressing oxidation of the barrier surface. No intentional doping was used, in order to avoid electrical cross-linking between the mesas. Reflection high energy electron diffraction (RHEED) analysis was used to monitor the crystalline quality of the barrier and contact layers to ensure relaxation – which could affect the bandstructure – did not occur. This was verified by a sharp, streaked RHEED reconstruction throughout growth. Finally, the contact layer was grown, with the same doping level as the absorption layer. For the sample grown on native GaSb, oxide desorption was carried out at 540 °C, followed by the growth of the GaSb buffer. The *nBn* overlayers were then grown under the same conditions that were used for the sample grown on GaAs. All growth rates were approximately 1.0 MLs^{-1}. In processing, both the upper and lower contacts were thermally evaporated using Ti/Au. TLM measurements were carried out, confirming low resistance, Ohmic contacts. Circular mesas with diameters between 25 – 800 μm were defined using standard photolithography and a citric-acid-based etchant. The mesas were defined without etching through the barrier layer (shallow etch) in order to suppress surface leakage currents, as noted above. It was found that only slight oxidation of the barrier layer surface – which remained

stable, even months after processing – occurred, as suppressed by the 10% Ga mole fraction. Potential problems with long term structural integrity and device reliability were therefore alleviated, particularly since encapsulation could be used where stability is essential over longer timescales. Dark current measurements were made using a Lakeshore TTPX low temperature probe station and Keithley 2400 and 6430 SourceMeters®. The probe station was equipped with a radiation shield, allowing for the exclusion of radiation incident from the 300 K scene. Spectral response was measured using a Nicolet 6700 Fourier Transform Infrared (FTIR) Spectrometer. An IR-563 blackbody was used to measure responsivity at a wavelength of 2.33 μm.

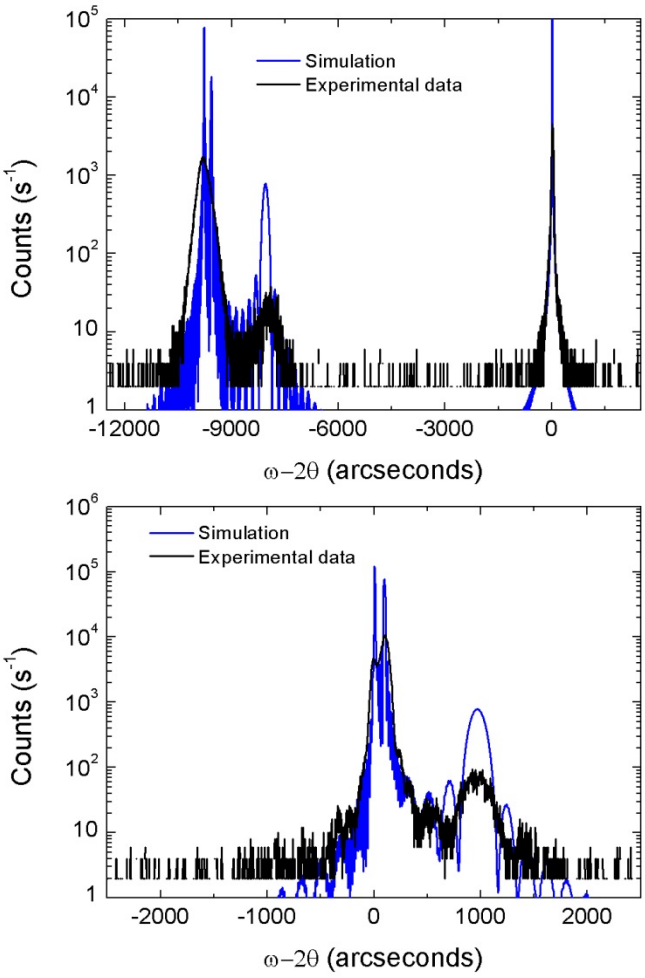

Figure 2: Measured and fitted XRD data for the two primary samples: (a) sample grown on GaAs, using an IMF array and (b) the sample grown on a native GaSb substrate.

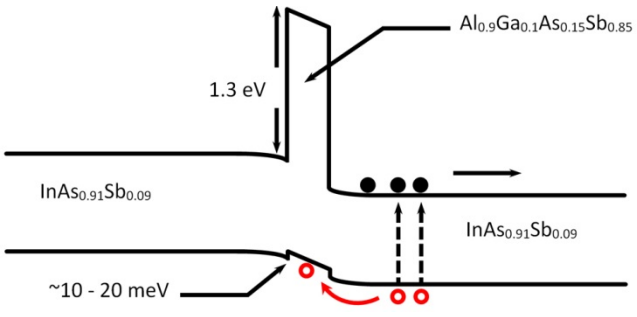

Figure 3: Approximate band diagram, as calculated according to the model of Krijn.17

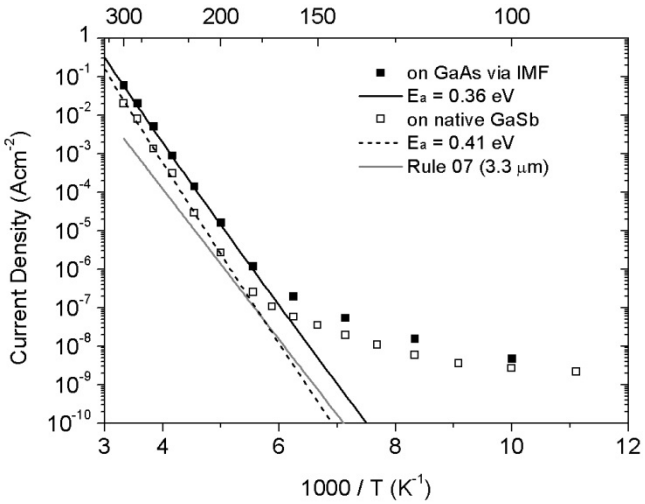

Figure 4: Arrhenius plots of the dark currents, at -0.1 V applied bias, for both primary samples. Activation energy fittings and a comparison with Rule 07 are also shown.

X-ray diffraction (XRD) scans were obtained using a Bede QC200 Diffractometer. Noise behaviour was analysed using a Stanford Research Systems SR570 Low Noise Preamplifier and an Agilent 35670A Dynamic Signal Analyser. An amplification level of 100 nAV^{-1} was used.

Fitted XRD scans for both primary samples are show in Figure 2. For the sample grown on a GaAs substrate, the full width at half maximum (FWHM) of the absorption layer peak (visible around -9800 arcsec) was ~300 arcsec. In contrast, the absorption layer peak for the sample grown on GaSb was 80 arcsec, indicating higher crystalline quality for this sample.

Features due to the barrier layers can also be seen at around -8000 arcsec, and around 1000 arcsec, respectively. For the sample grown on GaAs, no peak due to the GaSb buffer layer is seen (normally exhibited at -9,580 arcsec). This is due to the narrow thickness of the layer, i.e. the features are buried beneath the absorber peak (at -9800 arcsec). Details of the fitting parameters were given in Figure 1. Figure 3 shows an approximate band diagram for both samples, calculated using the model of Krijn.17 The model incorporates the effects of strain on the band positions. Arrhenius plots of the dark currents are shown in Figure 4. Inspecting the figure, it is immediately obvious that the two samples give similar levels of dark current performance, in spite of the lattice mismatch between the InAsSb absorption layer and the GaAs substrate and the lower crystalline quality (as inferred from the XRD FWHM of the absorption layer) for the growth on GaAs. This indicates the effective suppression of SRH generation by the *nBn* design: the surface threading dislocation densities under IMF growth – as known from transmission electron microscopy (TEM) measurements to be present at a level of around 10^8 cm^{-2} – are usually deleterious to device performance to a greater degree. Activation energy fittings were made using the following expression for the dark current density, J, in the diffusion current limited regime,

$$J \sim T^3 \exp\left(\frac{-Ea}{kT}\right) \qquad (1)$$

where Ea is the activation energy, k is the Boltzmann constant and the factor of T^3 accounts for the density of states. The results, as quoted in the figure, are close to the full intrinsic bandgap of the InAsSb absorption layers at zero temperature – predicted to be 0.35 eV according to the bowing parameter recommended by ref [18] – confirming diffusion limited dark currents. Note that the diffusion limited regime is indicated by correspondence with the low-temperature bandgap, rather than the bandgap at operating temperature.3 For the sample

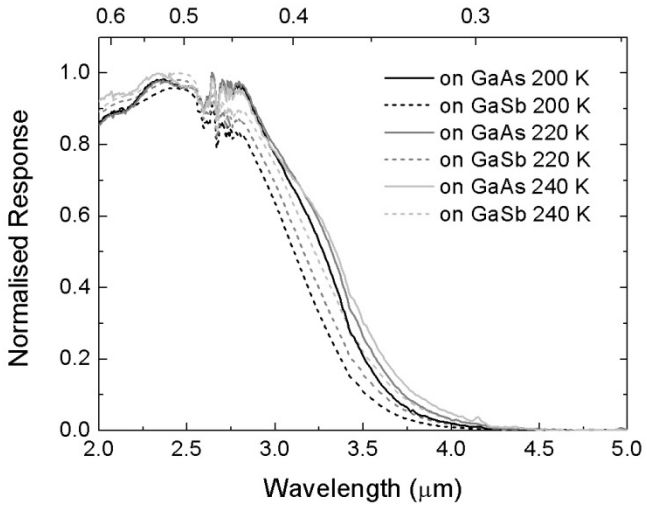

Figure 5: Spectral response for the primary samples for 200 – 240 K operating temperature. Solid lines: growth on GaAs (via IMF). Dashed lines: growth on native GaSb.

grown on GaSb, the activation energy is slightly larger than the intrinsic bandgap: this will be explained in terms of Moss Burstein shift in the subsequent text. A second gradient is visible for both samples between approximately 100 and 150 K. However, the gradient is too small (~0.1 eV) to indicate SRH recombination (i.e. significantly less than half the bandgap). Therefore, this region is likely to result from a shunt resistance associated with the barrier layer or band-to-band tunnelling currents associated with a small depleted volume of absorption layer material. Comparison is also made with Rule 07, an expression used to predict the dark current performance of an optimized HgCdTe detector for a given cut-off wavelength.19 In the figure, the Rule 07 cut-off wavelength parameter is listed as 3.3 μm: this corresponds to the 50% cut-off wavelength of our devices, as specified by the literature. Spectral response measurements are shown in Figure 5, indicating 200 K cut-off wavelengths of around 3.5 μm in each case. These cut-off wavelengths were determined by plotting the square of the photoresponse against energy and then extrapolating the low energy region to zero using a linear fit. It was noted that the responsivity experiences a gradual reduction in

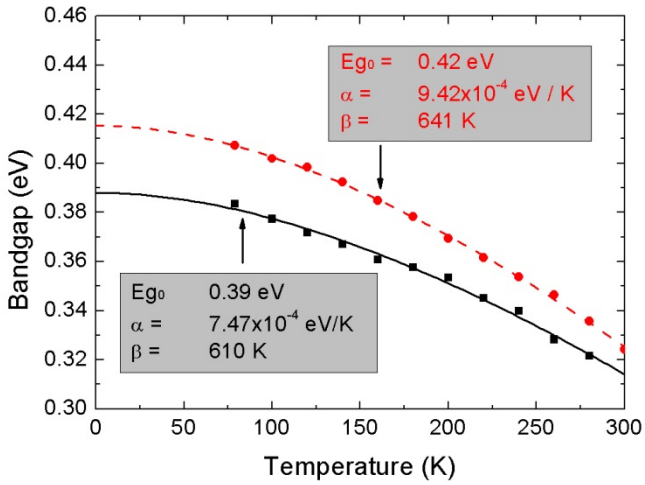

Figure 6: Absorber bandgap, as learned from the spectral response, plotted as a function of temperature for both primary samples. Growth on GaAs: (■). Growth on native GaSb: (•).

the region approaching cut-off: this effect could be reduced by using thicker absorption regions, resulting in larger absorption probabilities for longer-wavelength photons. The noted 3.5 μm cut-off is slightly shorter than expected, given that the InAsSb layers were grown with a composition lattice matched to GaSb. For example, ref [20] reports *nBn* detectors with an intrinsic $InAs_{0.91}Sb_{0.09}$ absorption layer and a cut-off wavelength of 4.2 μm at 200 K. This occurs as a result of Moss-Burstein shift due to the *n*-type doping in the absorption layers. This effect also results in a slightly larger than expected activation energy for the sample grown on GaSb, i.e. 0.41 eV rather than 0.35 eV. This activation energy figure corresponds closely with the measured bandgap from spectral response when extrapolated to zero-temperature using a Varshni fitting (~0.42 eV). The fitting is illustrated in Figure 6, together with a similar fitting for the sample grown on GaAs. Note that the bandgap for the sample grown on GaAs is slightly smaller than the bandgap for the sample grown on GaSb, owing to the increased Sb composition, as known from XRD measurements (see Figure 1). The direct correspondence between the bandgap and the activation energy confirms in each case that any potential barrier in the valence band between the absorption and barrier layers – occurring e.g. as a result of band-bending or strain relaxation – is either small or absent, or at

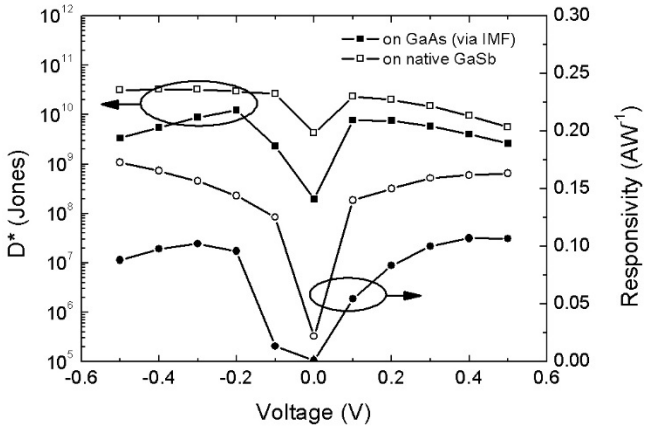

Figure 7: Shot-noise-limited D^* for both primary samples, as calculated using responsivity measurements made at 2.33 μm wavelength, for 200 K operating temperature.

least narrow enough that photogenerated holes can easily tunnel through it. Such a barrier would result in larger activation energies. With regards the choice of absorption layer doping density, it is worth pointing out that there is a trade-off between dark current performance, which is enhanced by heavy doping due to the pinning of the Fermi level at the conduction band edge – away from mid-gap traps – and quantum efficiency, which is degraded due to the reduction in the minority carrier lifetime. Responsivity measurements, taken at -0.2 V bias and 2.33 μm wavelength, yielded values of around 0.1 AW^{-1} and 0.15 AW^{-1} at for the sample grown on GaAs and the sample grown on native GaSb, respectively, at 200 K. The bias for optimal specific detectivity (D*) performance occurs between $-0.3 < V < 0.1$. This is typical for *nBn* detectors reported elsewhere.20 Figure 7 shows D^* as a function of bias for both samples. This was determined using the responsivity measurements plotted together with calculated noise values (for the high frequency limit). The calculated noise values were based upon the sum of the Shot noise and thermal noise from the dark current, together with a further Shot Noise contribution estimated by calculating the expected photocurrent due to absorption of 300 K background radiation (via the Planck Radiation formula), hence providing a more realistic estimate of real-world device performance. The calculated D^* figures

again show similar levels of performance regardless of the choice of substrate, with the difference being less than a factor of 3, although it should be noted that the sample grown on GaSb was found to be limited by the Shot noise originating from 300 K background photo-current at 200 K. These D* figures can also be compared with those for comparable HgCdTe detectors available commercially: ref [21] gives figures of 7×10^{10} Jones for a *p-i-n* device with a 3.4 μm cut-off wavelength at 210 K operating temperature. Comparing the results presented in Figure 7 with the above quoted figure, both samples achieve marginally lower D* figures-of-merit but have slightly longer cut-off wavelengths. It should further be pointed out that, in comparison with HgCdTe diodes, *nBn* sensors offer relatively straightforward growth and fabrication (and hence lower costs). Growth on GaAs also offers lower cost and larger area substrates. Responsivity measurements are also shown in the figure. It should be reiterated that the D* values were calculated subject to the proviso that the noise from the dark current is limited by Shot noise and thermal (Johnson) noise, rather than by 1/f noise. This may not be strictly true at low frequencies as will be investigated shortly. Furthermore, it should be noted that the optimum D* figure was obtained at a different bias to the optimum responsivity: for the sample grown on GaSb, the responsivity in

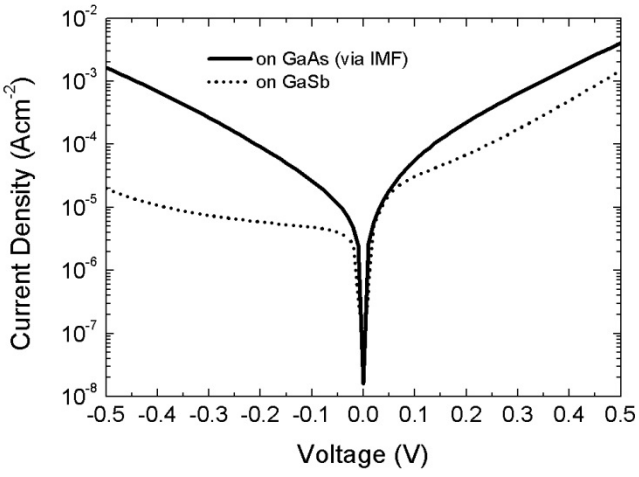

Figure 8: JV curves for both primary samples, measured with 300 K background radiation excluded, as used to calculate the D* figures of merit in Figure 7.

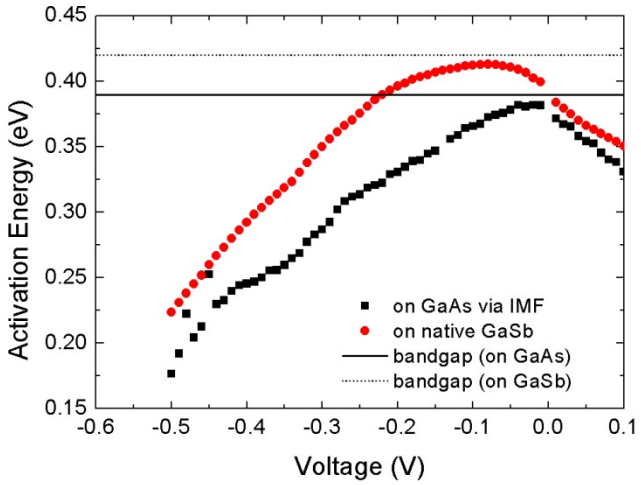

Figure 9: Activation energy behaviour for both primary samples as a function of bias, determined using Equation 1 using data between 220 – 300 K. The solid lines represent absorption layer bandgap values for zero temperature, as derived from Varhsni fittings.

fact peaks at a value slightly greater than 0.2 AW^{-1} at -0.9 V. However, the balance of factors affecting the D* is more favourable at small reverse bias, since the dark currents increase, and in fact become SRH limited, at larger reverse biases. Full, current density-voltage (JV) curves are shown in Figure 8 for both samples, as measured at 200 K. Figure 9 then shows activation energy behaviour as a function of bias. In each case, for the operational bias ranges quoted, the activation energies are close to the zero-temperature bandgap of the absorption layers, indicating diffusion limited behaviour, as noted above. However, with the application of larger reverse bias, smaller activation energies are exhibited, indicating that the SRH generation process begins to influence device performance.

A further study of the influence of the doping level in the absorption layer upon the cut-off wavelength and the dark current performance was then carried out. Two additional samples were grown under the same growth conditions used for the initial samples, but with reduced absorption layer doping of $\sim 9 \times 10^{16}$ cm^{-3}. Spectral response for these samples is shown in Figure 10. It can be seen that the cut-off wavelength is extended to approximately 4.1 μm at

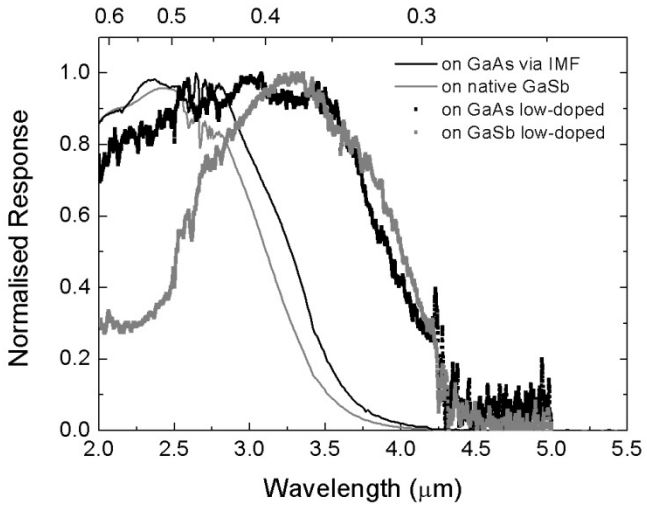

220

221 **Figure 10:** Spectral response measurements for an absorption layer doping of 4×10^{17} cm^{-3}

222 (primary samples) and 9×10^{16} cm^{-3} (low doped samples), as measured at 200 K.

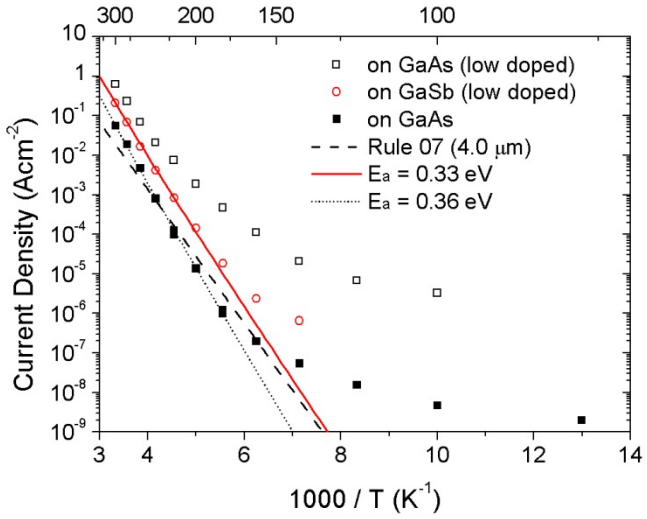

223

224 **Figure 11**: Arrhenius plots of the dark current density for absorption layer doping densities of

225 4×10^{17} cm^{-3} (primary sample grown on GaAs) and 9×10^{16} cm^{-3} (low doped samples).

226 A Rule 07 line is also shown.

227 200 K. This corresponds to a decrease in the bandgap of between 50 - 80 meV when comp-

228 ared to the samples with 4×10^{17} cm^{-3} absorption layer doping (i.e. the primary samples).

229 This is in good agreement with the change in the Fermi Energy between the two doping

230 levels (54 meV), as predicted by the literature,22 i.e. Moss Burstein shift is reduced. Figure

11 further shows Arrhenius plots for the two low-doped samples. Comparison is drawn with the primary (heavily doped) sample grown on GaAs. It can be seen that the sample grown on native GaSb has an activation energy of 0.3 eV, which is close to the expected low-temperature bandgap for low-doped $InAs_{0.91}Sb_{0.09}$ (0.35 eV), once again indicating diffusion limited dark currents. The slight reduction in the activation energy when compared to the higher-doped samples (0.36 – 0.41 eV) is attributed to a reduction in the Moss-Burstein effect, due to the lower dopant concentration, resulting in a smaller bandgap. However, the dark currents for the sample grown on GaAs are no longer observed to follow the diffusion limited gradient. It was thought that SRH generation was encouraged by the presence of extra threading dislocations under the IMF growth mode, the effects of which are no longer suppressed by Fermi level pinning due to heavy absorption layer doping. A Rule 07 line is also shown. The cut-off wavelength parameter was set to 4.0 μm, corresponding to the 50% cut-off wavelength of these devices, as learned from Figure 10.

Finally, noise performance was reviewed for the two primary samples. 1/f noise has previously been attributed to tunnelling through trap states and local modulations of carrier mobility.23 Noise spectra for the primary sample grown on GaAs are plotted in Figure 12 for temperatures between 240 – 300 K and a bias voltage of -0.2 V. Below 240 K, the measurement was dominated by the gain-bandwidth limit of the SR570 preamplifier. However, the resolution limit itself provides an indication of the noise performance: this instrumentation is well regarded for the performance of such measurements.24 Above 240 K, the noise “knee” frequencies (i.e. the frequencies at which the 1/f component is equal to component of the white noise at higher frequencies) can be seen to lie in the range 124 – 337 Hz. These can be compared with values from the literature of around 1 – 2 kHz for optimized photoconductive

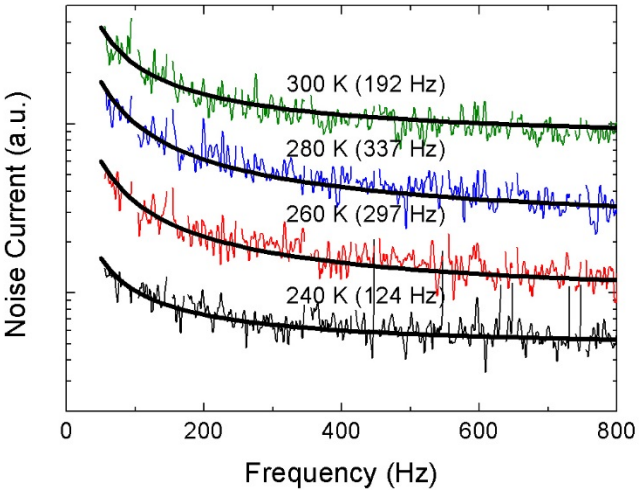

Figure 12: Noise frequency dependence, at -0.2 V bias, for the sample grown on GaAs with 4×10^{17} cm^{-3} absorption layer doping (primary sample). Knee frequencies are shown in brackets.

HgCdTe detectors operating in the MWIR, e.g. ref [25]. For the sample grown on native GaSb the noise knee frequency was determined to be less than 8 Hz, even at 300 K, as illustrated for -0.2 V bias in Figure 13. The lower knee frequency for this sample is likely attributable to the reduction in the number of defects due to the lattice matched growth. Such defects can cause the presence of trap states and hence influence the 1/f noise behaviour of the device.23 As a consequence of the above results, it can be stated that 1/f noise is not a concern for read-out-integrated circuits (ROICs) with integration times of less than 2 ms, or 125 ms, for the sample grown on GaAs and on GaSb, respectively.

In summary, InAsSb *nBn* detector structures were demonstrated both on GaAs, using an IMF array, and on native GaSb substrates. Similar levels of dark current performance were observed for the two cases, in spite of the lattice mismatch for sample grown on GaAs. Dark current activation energies, spectral response and D* measurements were analyzed at 200 K. Shot noise limited D* values greater than 10^{10} Jones noted for both samples. Two further samples

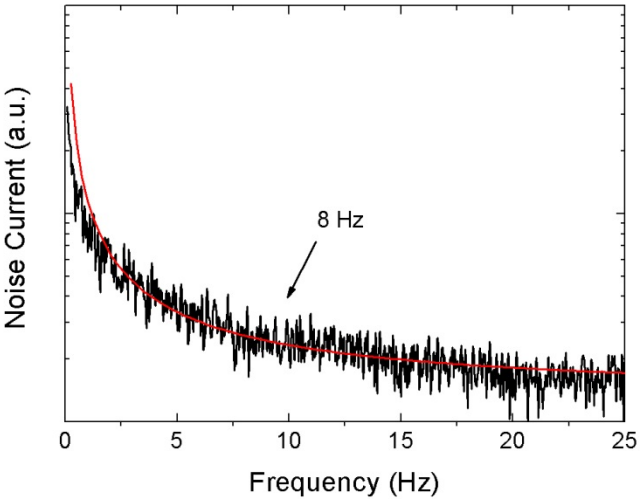

Figure 13: Noise frequency dependence, at -0.2 V bias, for the sample grown on GaSb with 4×10^{17} cm^{-3} absorption layer doping (primary sample), as measured at 300 K. The knee frequency is indicated in the figure.

were grown, again on GaAs and GaSb, respectively, with the same epilayer structure, but with lower absorption layer doping. It was found that the cut-off wavelength was extended, but that dark current performance was compromised for the sample grown on GaAs. Finally, noise spectral density measurements were made, showing noise knee frequencies lower than 350 Hz and 8 Hz, for the sample grown on GaAs and the sample grown on GaSb, respectively. Significantly, these measurements show that such detectors could be integrated with read-out integrated circuits (ROICs). Through operation at 200 K, operation with cost-effective thermoelectric coolers would also be possible.

The authors would like to thank the UK Engineering and Physical Sciences Research Council for the studentship provided to A. P. Craig (grant number EP/P505585/1) and the Royal Academy of Engineering for the fellowship awarded to A. R. J. Marshall (grant number EP/H043 993/1). Z.-B. Tian and S. Krishna would also like to acknowledge the support from the U.S. Air Force Research Laboratory under the contract FA9453-14-1-0248.

References

[1] S. Maimon and G. W. Wicks, Appl. Phys. Lett. 89, 151109 (2006).

[2] A. P. Craig, A. R. J. Marshall, Z.-B. Tian, S. Krishna and A. Krier, Appl Phys Lett 103, 253502 (2013).

[3] P. Klipstein, O. Klin, S. Grossman, N. Snapi, B. Yaakobovitz, M. Brumer, I. Lukomsky, D. Aronov, M. Yassen, B. Yofis, A. Glozman, T. Fishman, E. Berkowicz, O. Magen, I. Shtrichman, and E. Weiss, in Proc. SPIE 7660, Infrared Technology and Applications XXXVI, 76602Y (2010).

[4] M. Jain, G. Wicks, A. Marshall, A. Craig, T. Golding, K. Hossain, K. McEwan and C. Howle, in Proc. SPIE 9073, 907304 (2014).

[5] G. Bishop, E. Plis, J. B. Rodriguez, Y. D. Sharma, L. R. Dawson and S. Krishna, J. Vac. Sci. Technol. B 26(3), 1145 (2008).

[6] J. B. Rodriguez, E. Plis, G. Bishop, Y. D. Sharma, H. Kim, L. R. Dawson and S. Krishna, Appl. Phys. Lett. 91, 043514 (2007).

[7] E. Plis, J. B. Rodriguez, G. Balakrishnan, Y. D. Sharma, H. S. Kim, T. Rotter and S. Krishna, Semicond. Sci. Technol. 25 085010 (2010).

[8] A. Khoshakhlagh, J. B. Rodriguez, E. Plis, G. D. Bishop, Y. D. Sharma, H. S. Kim, L. R. Dawson, and S. Krishna, Appl. Phys. Lett. 91 263504 (2007).

[9] A. M. Itsuno, J. D. Phillips, and S. Velicu, Appl. Phys. Lett. 100, 161102 (2012).

[10] A.M. Itsuno, J.D. Phillips, and S. Velicu, J. Electron. Mater. 41, 2886–2892 (2012).

[11] I. M. Baker, S. S. Duncan and J. W. Copley, in Proc. SPIE 5406, 133 (2004).

[12] A. Krier and W. Suleiman, Semicond. Sci. Technol. 13, 950 (1998).

[13] P. C. Klipstein, Y. Gross, D. Aronov, M. ben Ezra, E. Berkowicz, Y. Cohen, R. Fraenkel, A. Glozman, S. Grossman, O. Klin, I. Lukomsky, T. Marlowitz, L. Shkedy, I. Shtrichman, N. Snapi, A. Tuito, M. Yassen and E. Weiss in Proc. SPIE 8704, Infrared

313 Technology and Applications XXXIX, 87041S (2013).
314 [14] S. H. Huang, G. Balakrishnan, A. Khoshakhlagh, A. Jallipalli, L. R. Dawson, and D. L.
315 Huffaker, Appl. Phys. Lett. 88, 131911 (2006).
316 [15] S. Huang, G. Balakrishnan, and D. L. Huffaker, J. Appl. Phys. 105, 103104 (2009).
317 [16] L. F. Luo, K. F. Longenbach and W. I. Wang, IEEE Electron Device Lett. 11, 12 (1990).
318 [17] M. P. C. M. Krijn, Semicond. Sci. Technol. 6, 27 (1991).
319 [18] I. Vurgaftman, J. R. Meyer, and L. R. Ram-Mohan, J. Appl. Phys., Vol. 89, 11 (2001).
320 [19] W. E. Tennant, D. Lee, M. Zandian, E. Piquette and M. Carmody, J. Electron. Mater. 37,
321 9 (2008).
322 [20] A. Soibel, C. J. Hill, S. A. Keo, L. Hoglund, R. Rosenberg, R. Kowalczyk, A.
323 Khoshakhlagh, A. Fisher, D. Z.-Y. Ting, and S. D. Gunapala, Appl Phys Lett 105, 023512
324 (2014).
325 [21] PV-2TE Series: “2 – 12 µm IR Photovoltaic Detectors Thermoelectrically Cooled”, Vigo
326 System S. A. (2015).
327 [22] P. K. Basu, “Theory of Optical Processes in Semiconductors”, Oxford University Press
328 (2007).
329 [23] F. N. Hooge, IEEE Trans. Electron Dev. 41, 11 (1994).
330 [24] C. Cismaru, M. Banbrook, P. J. Zampardi in International Conference on Compound
331 Semiconductor Manufacturing Technology, p289, May 14-17 (2007).
332 [25] R. Sewell, C.A. Musca, J.M. Dell, L. Faraone, K. Jozwikowski and A. Rogalski, J.
333 Electron. Mater. 32, 7 (2003).
334
335
336